

Time accelerated image super-resolution using shallow residual feature representative network

Meenu Ajith^{a,*}, Aswathy Rajendra Kurup^a, Manel Martínez-Ramón^a

^a*Department of Electrical and Computer Engineering, The University of New Mexico, New Mexico, 87106, USA*

Abstract

The recent advances in deep learning indicate significant progress in the field of single image super-resolution. With the advent of these techniques, high-resolution image with high peak signal to noise ratio (PSNR) and excellent perceptual quality can be reconstructed. The major challenges associated with existing deep convolutional neural networks are their computational complexity and time; the increasing depth of the networks, often result in high space complexity. To alleviate these issues, we developed an innovative shallow residual feature representative network (SRFRN) that uses a bicubic interpolated low-resolution image as input and residual representative units (RFR) which include serially stacked residual non-linear convolutions. Furthermore, the reconstruction of the high-resolution image is done by combining the output of the RFR units and the residual output from the bicubic interpolated LR image. Finally, multiple experiments have been performed on the benchmark datasets and the proposed model illustrates superior performance for higher scales. Besides, this model also exhibits faster execution time compared to all the existing approaches.

Keywords: Super-resolution, Convolutional neural networks, Residual learning

1. Introduction

Super-resolution (SR) is the process of enhancement of the resolution of an image where the high resolution (HR) image is estimated from its low resolution (LR) counterpart [1]. SR finds its application in many real-time problems from different fields such as microbiology [2], medical imaging [3], satellite imaging [4, 5] and in many Computer vision applications [6, 7].

*Corresponding author
Email address: majith@unm.edu (Meenu Ajith)

SR techniques can be classified into two broad classes based on the number of input images: Single input super-resolution (SISR) and multi-input super-resolution (MISR) [8]. SISR has an advantage over MISR in terms of its lower computational burden. Compared to the MISR techniques, which can improve the actual resolution by combining the information from different images, SISR techniques improve the image only perceptually, but this is often what the user needs. SISR techniques include algorithms that can be divided into three categories: methods based on interpolation such as bicubic interpolation [9], reconstruction based techniques [10, 11, 12] and learning-based methods that make use of machine learning techniques to learn from the training examples. Markov Random Field (MRF) [13], Neighbor embedding method, Manifold learning [14], sparse coding, Anchored regression [15] are a few learning-based techniques. Interpolation based methods are computationally inexpensive compared to the other two methods but they tend to show lower accuracy. Reconstruction based techniques can be time-consuming and their performance drops with the increase in the scale factor. Learning-based methods are known for their efficiency in both computation and performance [8]. Deep learning-based approaches are becoming more popular in this field due to their outstanding performance compared to other approaches. The traditional SR approaches are unable to remove the defects and artifacts due to compression while upscaling. Deep learning methods can solve this problem to a great extent [8]. Deep learning techniques have the advantage over other techniques due to their capability to extract high-level abstractions that help in getting a better mapping from LR space to HR space. Recently developed Convolutional neural network (CNN) and Generative adversarial network-based techniques have shown outstanding performance compared to the traditional approaches [1] but the main drawback of these approaches is their large training time and computational cost which makes these techniques hard to be implemented during a real-time scenario.

The main contributions of this paper are five-fold:

- We introduce a novel structure which stores residual information from the previous layers instead of the features themselves. The residual learning allows the network to avoid redundancies.
- The proposed shallow residual feature representative network (SRFRN) uses depthless convolutions resulting in a lightweight network. Hence in terms of training and testing time the network exhibits superior performance compared to the state-of-the-art networks.
- A patch extraction technique was used as pre-processing before passing the LR image into the network. This further reduced the time complexity of the model.
- In this work we introduce residual feature representative (RFR) units, which consist of convolutional blocks that help to extract features and store differential information.

- Finally, the network shows less degradation for higher scales. Therefore, different experiments conducted on various databases with $\times 4$ scale have shown outstanding performance compared to the existing approaches.

Different experiments have been conducted in order to measure the performance of our approach. Results show a significant advantage of the introduced methodology in terms of PSNR and computational time.

2. Related work

Over the years, several deep learning approaches have been implemented to address the SR problem. These approaches were mainly based on CNNs, of which, the first model was implemented by Dong et al. named Super-Resolution Convolutional Neural Network (SRCNN) which was inspired by the conventional Sparse-coding based SR methods [16]. The structure of SRCNN is fully feed-forward with learning upscaling filters and requires little pre and post-processing other than the optimization. SRCNN has the advantage of the simplicity of its structure [16] and good performance but the training time for this structure is very large. Further, in 2016, an accelerated version of SRCNN was introduced by Dong et al. named Fast Super-Resolution Convolutional Neural Networks (FSRCNN)[17]. This structure was implemented to address the time and computational complexity of SRCNN. FSRCNN was the first structure to use a deconvolutional layer for the reconstruction of HR from LR features. The structure was able to achieve a speed 40 times higher, superior accuracy and comparable image restoration quality to that of SRCNN [17]. The deconvolution layer makes use of nearest-neighbor interpolation while reconstructing which causes repetition of unsampled features in each direction [8]. Efficient sub-pixel convolution neural network (ESPCN) by Shi et al. tackles this problem by simplifying the deconvolution layer into sub-pixel convolution.[8, 18].

Apart from the smaller networks, several very deep networks were also used in SISR. One of the very first deep models was VDSR [19] which is a 20 weight layered VGG-net [20]. VDSR takes the bicubic interpolated image as input and the network learns to map from this interpolated image to the differential features between HR and bicubic. During training, different scale factors of the bicubic interpolated image are assembled. In 2016, Kim et al. [21] introduced the Deep recursive convolutional network (DRCN) that uses the same convolutional layer repeatedly as a result of which the number of parameters does not increase. The network uses the feature maps from each recursion to obtain a reconstructed high-resolution image (HR). The HR predictions from different levels of recursions were further combined to achieve a more accurate prediction. While fusing these HR outputs the scalar weights are not adaptive, that is, the scalar weights don't change with different inputs. DRCN and VDSR show similar performance except that DRCN uses a multi-supervised strategy for training. Due to their deep structure, they have a greater training time compared to other shallow structured networks. Eventually, the idea of residual units was incorporated into several networks. Residual units, in general, comprises of non-linear

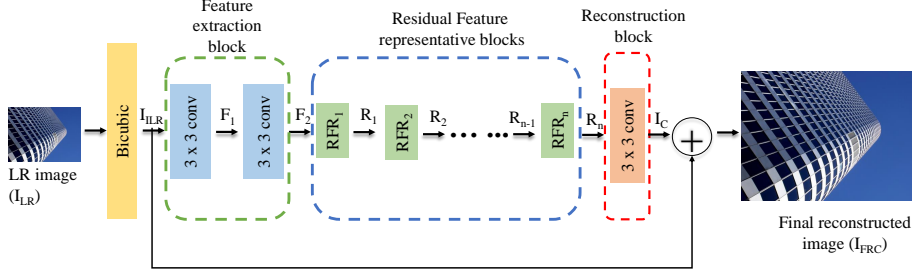


Figure 1: The architecture of the proposed approach.

convolutions and residual learning. SRResNet [1] inspired from ResNet [22] was the first network to implement these residual units and it focused on reconstructing photo-realistic textures from LR images. Later on, the Deep Recursive residual network (DRRN) was proposed by Tai et al. which used the technique of residual learning and recursive blocks to control model parameters and to tackle training difficulty [23]. Residual dense network (RDN)[24] proposed by Zhang et al. make use of hierarchical features from the convolutional layers to perform SR. The basic units used here are the densely connected Residual dense blocks (RDB). The main function of RDB is to extract dense local features. The local features are further combined globally using dense connections and residual learning. Progressive property of ResNet has been adopted in the DEGREE [25] which combined it with the sub-band reconstruction technique used in traditional methods. The high-frequency details were reconstructed using a recursive residual block. Another such network that makes use of this progressive property is the Laplacian Pyramid Super-Resolution Network (LapSRN) [26]. These networks don't use bicubic interpolation as the initial step and the progressive reconstruction is applied to multi-scale HR predictions. The deeper nature of the structure poses training difficulties in terms of a large number of parameters, especially for larger scales.

3. Proposed Approach

The structure of SRFRN consists of four parts as shown in Fig 1: bicubic interpolation block, feature extraction blocks, residual feature representative blocks, and a reconstruction block. Let I_{LR} and I_{HR} denote the input LR image and the ground truth HR image. Initially, the bicubic block is used to

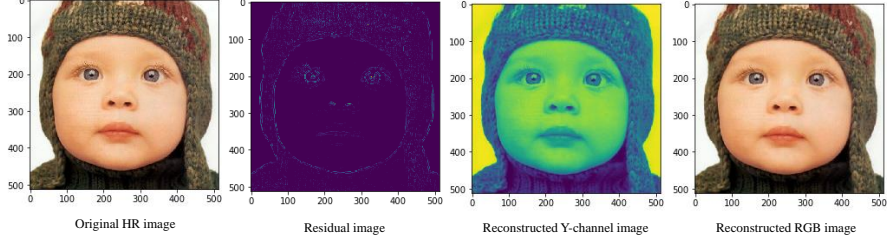


Figure 2: The original HR image and other image representations extracted from the model.

upsample the input LR image and the resulting image is passed onto the next block.

$$I_{ILR} = B(I_{LR}) \quad (1)$$

where I_{ILR} denotes the interpolated LR image and $B(\cdot)$ represents the bicubic interpolation operation. This predefined up sampling helps in the modeling of image details and creates an interpolated image of the required size. The definitive knowledge of the domain is highly beneficial for the following convolutional blocks. Moreover, similar structures have been used in several super-resolution structures [27, 28]. Next, the feature extraction block consists of two convolutional layers with 64 filters each and a kernel size of 3×3 . This block outputs the feature maps of the upsampled image. The convolutional layers that extract the features can be formulated as follows:

$$F_1 = W_1 * I_{ILR} + B_1 \quad (2)$$

$$F_2 = W_2 * F_1 + B_2 \quad (3)$$

where $*$ is the convolution operator.

Here F_1 and F_2 represents the features extracted from the first and second layers of the feature extraction block. Further, the filters are denoted as W_1 and W_2 and the respective biases are B_1 and B_2 . The feature extraction block is followed by a series of residual feature representative blocks (RFR). The network is capable of accommodating n RFR units and each of them consists of 3 convolutional blocks that use a kernel of size 3×3 . The output from the n^{th} RFR block can be represented as follows:

$$R_n = f_{RFR_n}(R_{n-1}) \quad (4)$$

where $f_{RFR_n}(\cdot)$ is a function consisting of convolutions and leaky rectified linear units [29]. The RFR units are designed to work based on residual learning. This technique was employed to enhance the memory of the network and to combine information from the former convolutional blocks.

Finally, in the reconstruction block, another 3×3 convolution is performed on the hierarchical features extracted from the RFR units. A feature fusion

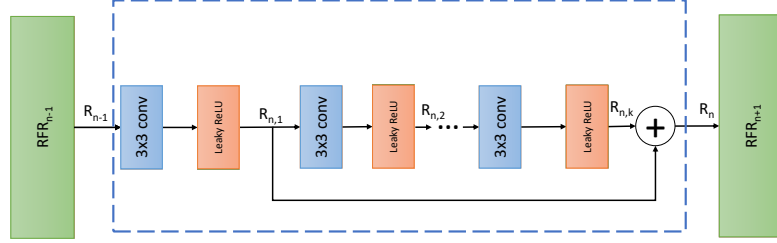


Figure 3: Residual feature representative blocks

method is employed as the last step and the output from the reconstruction layer is concatenated with the output of the bicubic interpolation block from the initial stage. The predicted HR image from the proposed model can be expressed as follows:

$$I_{FRC} = I_{ILR} + I_C \quad (5)$$

where I_{FRC} and I_C represents the final reconstructed output and the convolutional output.

3.1. Residual Representative Block

The residual learning-based CNN has been proven to more powerful than the non-residual networks in several works related to SR [30, 31, 32, 33]. The RFR blocks used in this work consist of a series of shallow convolutional layers stacked together. Additionally, each of the convolutional layers is followed by a Leaky ReLU activation function. The Leaky ReLU is used over ReLU since the latter gets saturated at the negative area and hence the gradient becomes zero. If this happens, the training stalls in these neurons during the backpropagation step. The output of the n^{th} RFR block can be expanded and formulated as:

$$R_n = R_{n,k} + R_{n,1} \quad (6)$$

$$R_{n,1} = \max \left\{ 0.1(W_{n,1} * R_{(n-1),1} + B_{n,1}), (W_{n,1} * R_{(n-1),1} + B_{n,1}) \right\} \quad (7)$$

$$R_{n,k} = \max \left\{ (0.1(W_{n,k} * R_{(n-1),(k-1)} + B_{n,k}), (W_{n,k} * R_{(n-1),(k-1)} + B_{n,k})) \right\} \quad (8)$$

where $R_{n,k}$ and $R_{n,1}$ denote the output of the 1_{st} and k _{th} convolutional layers of the given RFR block. Here R_n also represents the feature fusion at the end of each RFR block. This technique helps in significant improvement in information flow. Finally, it also acts as a local error-correcting feedback system to accelerate the training and thereby resulting in faster convergence. Since the basic blocks of RFR consist of standard convolutional units that are not deep, this structure is easily trainable, and its depth can be reduced without compromising the PSNR. The detailed structure is further illustrated in Fig. 3

3.2. Loss Function

In the super-resolution problem, several loss functions were introduced to minimize the reconstruction error of the generated HR image. The most common amongst them is the pixel-wise L1 and L2 loss. The sum of all the absolute errors between each pixel in the reconstructed and ground truth HR image is calculated to obtain the L1 loss. Meanwhile, the L2 loss was unable to provide high-quality reconstruction images and often lead to smooth and blurry textures in them. Further, the convergence rate of L1 loss was much faster compared to the L2 loss. Thus, minimizing the L1 loss results in a relatively high peak signal to noise ratio (PSNR) with less complexity. But the main disadvantage of the pixel-wise loss function is that it does not improve the visual perception of the generated image. In order to alleviate this issue, several other loss functions such as content loss [34], adversarial loss [35] and texture loss [36] were introduced. Though they succeeded in improving the perceptual quality, the computational complexity was comparatively high. Since the PSNR improvement was not significant in our experiments, in this work we only consider the L1 loss, which is relatively less complex. Hence the optimization of the proposed model is done by minimizing the difference between the ground truth I_{HR} and the predicted image I_{FRC} . This error minimization is formulated as follows:

$$L1 = \frac{1}{N} \sum_{i=1}^N \|I_{FRC} - I_{HR}\|_1 \quad (9)$$

4. Experiments

4.1. Databases

The training of this model was conducted on two datasets and it utilized 200 images from the Berkeley Segmentation Dataset (BSD) [37] and 91 images from Yang dataset [38]. Data augmentation methods such as rotation, flipping, and scaling were done to increase the training data to 2328 images. Further, the testing was done on four widely used datasets: Set5 [39], Set14 [40], BSD100 [41] and Urban100 [42]. These databases include various natural and urban scenes from diverse environments. Here the performance evaluation with peak signal-to-noise ratio (PSNR) and structural similarity (SSIM) [43] is done only on the luminance channel (Y channel) of the YCbCr color space.

Scale	Model	Set5 PSNR/SSIM	Set14 PSNR/SSIM	BSD100 PSNR/SSIM	Urban100 PSNR/SSIM
2	Bicubic	33.66/0.9299	30.24/0.8688	29.56/0.8431	26.88/0.8403
	SRCNN	36.66/0.9542	32.42/0.9063	31.36/0.8879	29.50/0.8946
	FSRCNN	36.99/0.9550	32.73/0.909	31.51/0.8910	29.87/0.9010
	VDSR	37.53/0.9587	33.03/0.9124	31.90/0.8960	30.76/0.9140
	LapSRN	37.52/0.9592	33.08/0.9132	31.80/0.8958	30.41/0.9101
	RDN	38.24 /0.9614	34.01/0.9212	32.34/0.9017	32.89 /0.9353
	SRFRN (ours)	36.58/ 0.9635	34.18 / 0.9317	33.57 / 0.9133	32.67/ 0.9337
3	Bicubic	30.39/0.8682	27.55/0.7742	27.21/0.7385	24.46/0.7349
	SRCNN	32.75/0.9090	29.28/0.8209	28.41/0.7863	26.44/0.8088
	FSRCNN	33.16/0.9140	29.42/0.8242	28.52/0.7893	26.41/0.8064
	VDSR	33.66/0.9213	29.77/0.8314	28.82/0.7976	27.14/0.8279
	LapSRN	33.78/0.9214	29.87/0.8333	28.81/0.7970	27.06/0.8270
	RDN	34.71 /0.9296	30.57/0.8468	29.26/0.8093	28.80/0.8653
	SRFRN (ours)	34.30/ 0.9336	32.77 / 0.8552	32.38 / 0.8226	31.40 / 0.8669
4	Bicubic	28.42/0.8104	26.00/0.7027	25.96/0.6675	23.14/0.6577
	SRCNN	30.48/0.8628	27.49/0.7503	26.90/0.7101	24.79/0.7374
	FSRCNN	30.71/0.8650	27.70/0.7560	26.97/0.7140	24.61/0.7271
	VDSR	31.35/0.8838	28.01/0.7674	27.29/0.7251	25.18/0.7524
	LapSRN	31.54/0.8850	28.19/0.7720	27.32/0.7281	25.21/0.7563
	RDN	32.47/0.8990	28.81/0.7871	27.72/0.7419	26.61/ 0.8028
	SRFRN (ours)	33.14 / 0.9137	31.95 / 0.7931	31.77 / 0.7522	30.74 /0.7998

Table 1: Comparison of average PSNR(dB) and SSIM among the CNN-based methods and bicubic interpolation on test datasets Set5, Set14, B100 , and Urban100 for scale factor $\times 2$, $\times 3$, $\times 4$.

4.2. Training

The proposed SRFRN model was trained on 2328 images with a 6-layer deep convolutional architecture. The different scaling factors considered are 2, 3 and 4 and the downsampling was done using bicubic interpolation. To accelerate the training process, a patch extraction technique was employed as a preprocessing technique. At first, smaller patches of sub-images were extracted from the given HR images. A patch size of $m \times n$, much smaller than the minimum image size in the dataset was utilized to minimize the computational burden. These patches were further downsampled to create the corresponding LR sub-images. Hence the entire training was conducted using these sub-images with a batch size of 24. The learning rate for training is originally fixed to 10^{-3} and is decreased if the validation error does not change for successive 10 epochs. The model uses the Adam optimizer [44] and the loss function for optimizing this network is the mean absolute error or L1. The proposed model is trained for 50 iterations to obtain the optimal parameters and the total training time is 20 minutes on an NVIDIA GeForce GTX 1060 GDDR5 GPU.

5. Results

5.1. Comparison with the State-of the Art Methods

In this section, we provide a comparison of the proposed approach with bicubic interpolation and various other CNN based methods. This quantitative

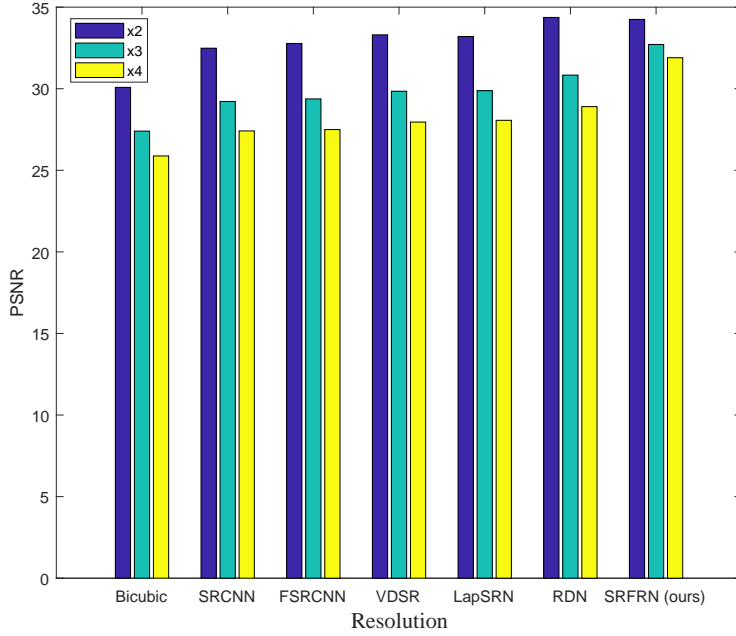


Figure 4: Comparison of the average PSNR of all methods for different resolutions.

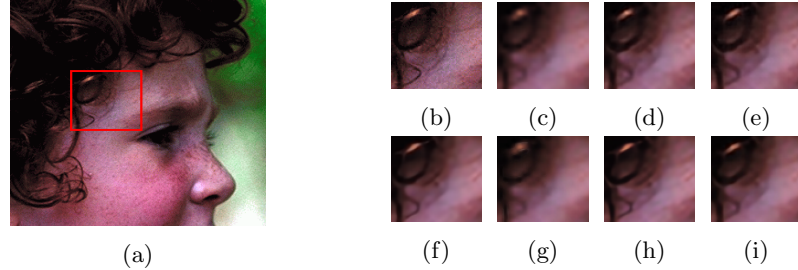


Figure 4: Image super resolution with scale $\times 3$. (a) Set5:img_004, (b) HR, (c) Bicubic, (d) SRCNN, (e) FSRCNN, (f) LapSRN, (g) VDSR, (h) RDN and (i) SRFRN (ours).

measure is based on two evaluation metrics such as PSNR and SSIM. Based on this, different experiments were conducted on $\times 2$, $\times 3$ and $\times 4$ scales to examine the performance of the proposed algorithm. Table 1 demonstrates the super resolving ability of various approaches such as SRCNN [16], FSRCNN [17], VDSR [19], LapSRN [26], RDN [24], bicubic interpolation, and our model. The superior performance of the proposed approach is mainly attributed to the residual learning mechanism as well as the shallow nature of the convolutions. Though our approach shows a nominal decrease in PSNR for $\times 2$ scales in the case of the Set5 database, the result cannot be generalized since the test database has only 5 images. In contrast, it was observed that for higher scale factors such as $\times 3$ and $\times 4$, the proposed approach shows a significant rise in

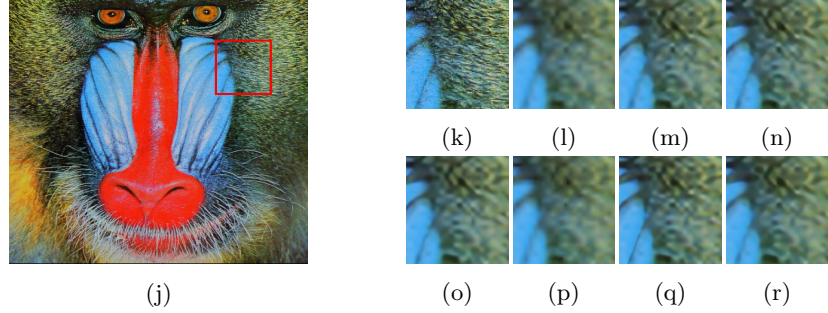


Figure 4: Image super resolution with scale $\times 3$. (a) Set14:img_001, (b) HR, (c) Bicubic, (d) SRCNN, (e) FSRCNN, (f) LapSRN, (g) VDSR, (h) RDN and (i) SRFRN (ours).

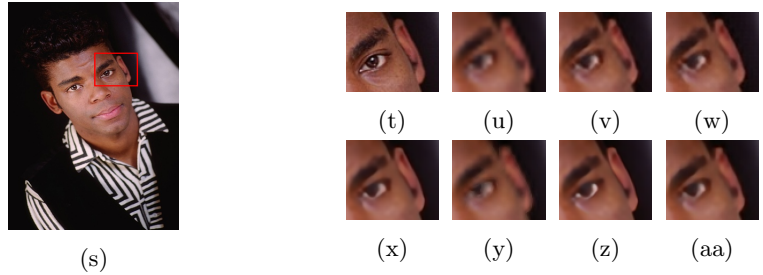


Figure 4: Image super resolution with scale $\times 4$. (a) BSD100:img_063, (b) HR, (c) Bicubic, (d) SRCNN, (e) FSRCNN, (f) LapSRN, (g) VDSR, (h) RDN and (i) SRFRN (ours).

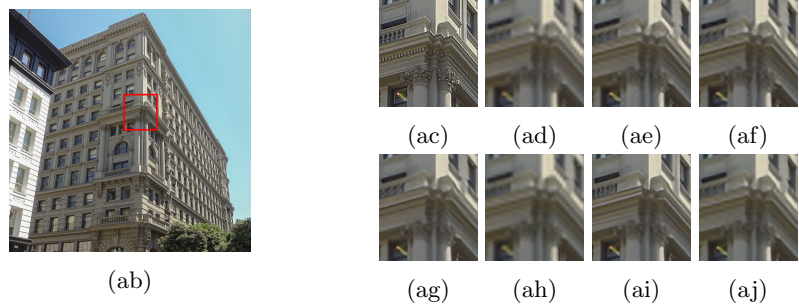


Figure 4: Image super resolution with scale $\times 4$, (a) Urban100:img_014, (b) HR, (c) Bicubic, (d) SRCNN, (e) FSRCNN, (f) LapSRN, (g) VDSR, (h) RDN and (i) SRFRN (ours).

PSNR compared to the rest of the state-of-the-art approaches. Further, the most significant increase (4.13 dB) in PSNR for an upscaling factor of 4 can be noted in the Urban100 database with 100 test images. When compared to our approach most of the benchmark algorithms tend to fail at higher scale factors for all the test databases. Besides, Fig. 4 shows the comparison of the average PSNR for all the methods in various scales. The traditional CNN based methods exhibit a minimal increase in PSNR compared to each other whereas the

proposed method outperforms all of them with a higher margin of PSNR for all the different resolutions.

Fig. 4, 4, 4 and 4 shows the perceptual quality analysis on Set 5, Set 14, BSD100 and Urban100 test databases. The visual comparison with the benchmark algorithms for scales $\times 3$ and $\times 4$ are illustrated using these results. Also, the proposed approach has relatively lesser artifacts and obtains clear edges.

5.2. Training and Test time Analysis

The time and space complexity of the proposed model is evaluated by determining the number of parameters and the test time. Table 2 presents the comparison of computational time for an upscaling factor of 4 for the various deep learning methods. Firstly, it is observed that the proposed approach reaches convergence much faster than state-of-the-art methods. In the case of SRCNN, one of the simplest models, it takes 3 days to train even with 12 times lesser parameters compared to the proposed approach. Additionally, with a greater number of parameters, there is a significant increase in training time (1-6 days) for models such as LapSRN, DRRN [23], DRCN [21] and RDN. Another model that takes lesser training time is VDSR, but it still has higher test time and low PSNR like SRCNN. In the case of deeper models such as DRRN and DRCN, the test time is more than 1 minute and hence they are impractical to be used in real-time with the hardware available for the experiments. It should be noted that, even though FSRCNN has the least number of learnable parameters, its test time is not significantly different compared to the proposed approach. Hence both approaches have superior time efficiency and cost less memory. But in terms of PSNR and training time, our model achieves better performance than FSRCNN. Hence in overall, the computational complexity of our model is the least compared to the rest of the CNN based approaches. Fig. 5 on the other hand demonstrates the test time for all the databases used in the evaluation of the proposed approach. It can be seen that the test time is comparatively very less and there is only slight variation even when we use higher scales.

Models	PSNR/SSIM (x4)	Train data	Parameters	Test time	Train time
SRCNN	30.48/0.8628	ImageNet database	57K	0.180	3 days
FSRCNN	30.71/0.8657	G200 + Yang91	12K	0.015	few hours
VDSR	31.35/0.8838	G200 + Yang91	665K	0.120	4 hours
LapSRN	31.54/0.8850	G200 + Yang91	812K	0.200	3 days
DRRN	31.68/0.8888	G200 + Yang91	297K	1.210	4 days
DRCN	31.53/0.8854	Yang91	1.77M	1.82	6 days
RDN	32.47/0.8990	DIV2K	22M	1.56	1 day
SRFRN (ours)	33.18/0.8488	G200 + Yang91	702K	0.041	20 min

Table 2: Computational complexity of the different CNN based models.

5.3. PSNR Vs Number of RFR Blocks

Fig. 6 and Table 3 illustrates the variation in PSNR with the increase in the number of RFR blocks. In the proposed model, the number of learnable

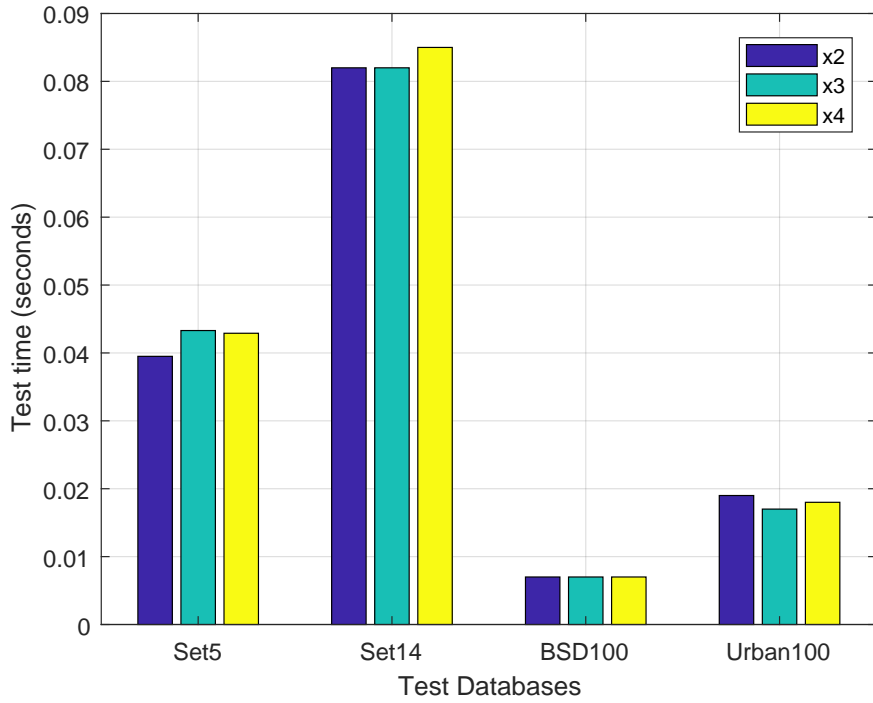


Figure 5: Comparison of test time for different databases and scales for the proposed approach.

parameters is directly proportional to the number of RFR blocks. The most significant change in PSNR occurs when the number of RFR blocks changes from 1 to 2. Later, the PSNR value in the graph converges by reaching the peak value and then reduces with the increase in the number of RFR blocks. From the table it can be observed that with just 2 RFR blocks the model was able to achieve a PSNR of 36.31, thereby reducing the time complexity. In the following experiments, the highest PSNR of 36.58 was computed using 6 RFR blocks. Thus, the graph illustrates the tradeoff between the number of parameters and PSNR. Finally, the performance of the model drops and the system converges when 7 or more RFR blocks are used.

Number of RFR blocks	1	2	3	4	5	6	7
Number of parameters	148K	259K	370K	481K	592K	702K	813K
PSNR (dB)	35.79	36.31	36.39	36.5	36.52	36.58	36.53

Table 3: Variation of PSNR in accordance with number of parameters and RFR blocks.

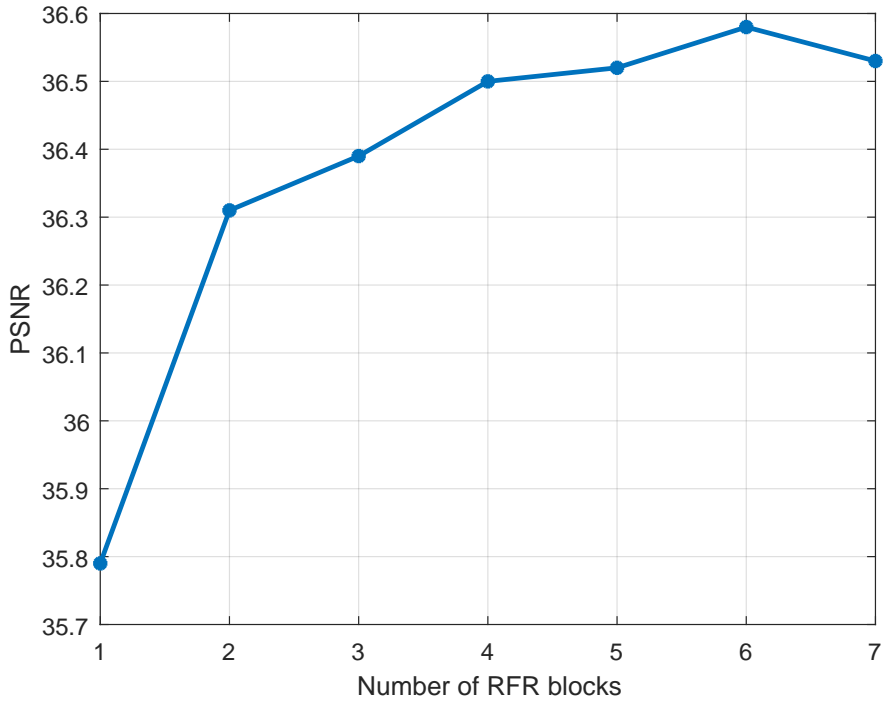


Figure 6: Plot of number of RFR blocks vs PSNR for scale 2.

6. Conclusion

Super-resolution is a tool of interest in many applications namely, remote sensing, medical applications, entertainment, where these techniques are intended to improve the user experience. In all these applications, besides reconstruction performance, high speed is required, mainly in those applications that demand real-time execution. In this work, we introduced a novel structure for SISR that uses a bicubic interpolated image followed by a set of blocks constructed by a novel structure consisting of convolutional blocks interleaved with feed-forward residual information (RFR units). The bicubic interpolated image is added to the output of the last block to allow the chain of RFR blocks to process differential information. The effect is that the RFR residuals correct the bicubic interpolated image. Further, the training speed is of about 20 minutes, compared to a few hours or days for the state-of-the-art methods, and the test time is on average 41 ms, only worse than the FSRCNN, whose test time is 15 ms. The rest of the methods have a test time 10 to 200 times slower. The reasons for this speed improvement are two. First, the structure uses simpler convolutional blocks, which make the training much faster compared to those structures with deeper and more complex convolutional blocks. Second, the method is based on the construction of residual features, which hold information related only to the interpolation error, not about the image itself, which requires lesser training epochs. Additionally, while testing with $\times 2$

scale, the average PSNR of our structure exceeds more than 2dB those of the other methodologies except in the case of RDN. Nevertheless, when the scale is increased, our method shows a lower degradation in PSNR, which is 1.5 dB, compared to the 4 to 5 dB of the average degradation of the rest of the methods. The results show that the accuracy of the introduced architecture is competitive or better than the accuracies shown by the state-of-the-art methods tested in this work.

7. Acknowledgments

Authors would like to thank UNM Center for Advanced Research Computing for providing high performance computing, large-scale storage and visualization resources.

References

- [1] C. Ledig, L. Theis, F. Huszár, J. Caballero, A. Cunningham, A. Acosta, A. Aitken, A. Tejani, J. Totz, Z. Wang, et al., Photo-realistic single image super-resolution using a generative adversarial network, in: Proceedings of the IEEE conference on computer vision and pattern recognition, 2017, pp. 4681–4690.
- [2] E. F. Fornasiero, F. Opazo, Super-resolution imaging for cell biologists: Concepts, applications, current challenges and developments, *Bioessays* 37 (4) (2015) 436–451.
- [3] M. D. Robinson, S. J. Chiu, C. A. Toth, J. A. Izatt, J. Y. Lo, S. Farsiu, New applications of super-resolution in medical imaging, in: *Super-Resolution Imaging*, CRC Press, 2017, pp. 401–430.
- [4] C. H. Genitha, K. Vani, Super resolution mapping of satellite images using hopfield neural networks, in: *Recent Advances in Space Technology Services and Climate Change 2010 (RSTS & CC-2010)*, IEEE, 2010, pp. 114–118.
- [5] H. Zhang, Z. Yang, L. Zhang, H. Shen, Super-resolution reconstruction for multi-angle remote sensing images considering resolution differences, *Remote Sensing* 6 (1) (2014) 637–657.
- [6] R. Yeh, C. Chen, T. Y. Lim, M. Hasegawa-Johnson, M. N. Do, Semantic image inpainting with perceptual and contextual losses, *arXiv preprint arXiv:1607.07539* 2 (2016) 3.
- [7] K. Nasrollahi, T. B. Moeslund, Super-resolution: a comprehensive survey, *Machine vision and applications* 25 (6) (2014) 1423–1468.
- [8] W. Yang, X. Zhang, Y. Tian, W. Wang, J.-H. Xue, Q. Liao, Deep learning for single image super-resolution: A brief review, *IEEE Transactions on Multimedia*.

- [9] R. Keys, Cubic convolution interpolation for digital image processing, *IEEE transactions on acoustics, speech, and signal processing* 29 (6) (1981) 1153–1160.
- [10] C. Douchon, Lanczos filtering in one and two dimensions j, *Appl. Meterology* 18 (1979) 1016–22.
- [11] J. Sun, Z. Xu, H.-Y. Shum, Image super-resolution using gradient profile prior, in: *2008 IEEE Conference on Computer Vision and Pattern Recognition*, IEEE, 2008, pp. 1–8.
- [12] Q. Yan, Y. Xu, X. Yang, T. Q. Nguyen, Single image superresolution based on gradient profile sharpness, *IEEE Transactions on Image Processing* 24 (10) (2015) 3187–3202.
- [13] W. T. Freeman, T. R. Jones, E. C. Pasztor, Example-based super-resolution, *IEEE Computer graphics and Applications* (2) (2002) 56–65.
- [14] H. Chang, D.-Y. Yeung, Y. Xiong, Super-resolution through neighbor embedding, in: *Proceedings of the 2004 IEEE Computer Society Conference on Computer Vision and Pattern Recognition, 2004. CVPR 2004.*, Vol. 1, IEEE, 2004, pp. I–I.
- [15] J. Salvador, *Example-Based Super Resolution*, Academic Press, 2016.
- [16] C. Dong, C. C. Loy, K. He, X. Tang, Learning a deep convolutional network for image super-resolution, in: *European conference on computer vision*, Springer, 2014, pp. 184–199.
- [17] C. Dong, C. C. Loy, X. Tang, Accelerating the super-resolution convolutional neural network, in: *European conference on computer vision*, Springer, 2016, pp. 391–407.
- [18] W. Shi, J. Caballero, F. Huszár, J. Totz, A. P. Aitken, R. Bishop, D. Rueckert, Z. Wang, Real-time single image and video super-resolution using an efficient sub-pixel convolutional neural network, in: *Proceedings of the IEEE conference on computer vision and pattern recognition, 2016*, pp. 1874–1883.
- [19] J. Kim, J. Kwon Lee, K. Mu Lee, Accurate image super-resolution using very deep convolutional networks, in: *Proceedings of the IEEE conference on computer vision and pattern recognition, 2016*, pp. 1646–1654.
- [20] A. Veit, M. J. Wilber, S. Belongie, Residual networks behave like ensembles of relatively shallow networks, in: *Advances in neural information processing systems*, 2016, pp. 550–558.
- [21] J. Kim, J. Kwon Lee, K. Mu Lee, Deeply-recursive convolutional network for image super-resolution, in: *The IEEE Conference on Computer Vision and Pattern Recognition (CVPR)*, 2016.

- [22] K. He, X. Zhang, S. Ren, J. Sun, Identity mappings in deep residual networks, in: European conference on computer vision, Springer, 2016, pp. 630–645.
- [23] Y. Tai, J. Yang, X. Liu, Image super-resolution via deep recursive residual network, in: 2017 IEEE Conference on Computer Vision and Pattern Recognition (CVPR), 2017, pp. 2790–2798.
- [24] Y. Zhang, Y. Tian, Y. Kong, B. Zhong, Y. Fu, Residual dense network for image super-resolution, in: Proceedings of the IEEE conference on computer vision and pattern recognition, 2018, pp. 2472–2481.
- [25] W. Yang, J. Feng, J. Yang, F. Zhao, J. Liu, Z. Guo, S. Yan, Deep edge guided recurrent residual learning for image super-resolution, *IEEE Transactions on Image Processing* 26 (12) (2017) 5895–5907.
- [26] W.-S. Lai, J.-B. Huang, N. Ahuja, M.-H. Yang, Deep laplacian pyramid networks for fast and accurate super-resolution, in: Proceedings of the IEEE conference on computer vision and pattern recognition, 2017, pp. 624–632.
- [27] R. Timofte, V. De Smet, L. Van Gool, Anchored neighborhood regression for fast example-based super-resolution, in: The IEEE International Conference on Computer Vision (ICCV), 2013.
- [28] M. Bevilacqua, A. Roumy, C. Guillemot, M. line Alberi Morel, Low-complexity single-image super-resolution based on nonnegative neighbor embedding, in: Proceedings of the British Machine Vision Conference, BMVA Press, 2012, pp. 135.1–135.10. doi:<http://dx.doi.org/10.5244/C.26.135>.
- [29] A. L. Maas, A. Y. Hannun, A. Y. Ng, Rectifier nonlinearities improve neural network acoustic models, in: in ICML Workshop on Deep Learning for Audio, Speech and Language Processing, 2013.
- [30] B. Lim, S. Son, H. Kim, S. Nah, K. M. Lee, Enhanced deep residual networks for single image super-resolution, 2017 IEEE Conference on Computer Vision and Pattern Recognition Workshops (CVPRW) (2017) 1132–1140.
- [31] C. Szegedy, S. Ioffe, V. Vanhoucke, A. A. Alemi, Inception-v4, inception-resnet and the impact of residual connections on learning, in: Proceedings of the Thirty-First AAAI Conference on Artificial Intelligence, AAAI17, AAAI Press, 2017, p. 42784284.
- [32] J. Kim, J. K. Lee, K. M. Lee, Accurate image super-resolution using very deep convolutional networks, 2016 IEEE Conference on Computer Vision and Pattern Recognition (CVPR) (2015) 1646–1654.

- [33] K. Zhang, W. Zuo, S. Gu, L. Zhang, Learning deep cnn denoiser prior for image restoration., in: IEEE Conference on Computer Vision and Pattern Recognition, Vol. abs/1704.03264, 2017.
- [34] J. Johnson, A. Alahi, L. Fei-Fei, Perceptual losses for real-time style transfer and super-resolution, in: European Conference on Computer Vision, 2016.
- [35] I. Goodfellow, J. Pouget-Abadie, M. Mirza, B. Xu, D. Warde-Farley, S. Ozair, A. Courville, Y. Bengio, Generative adversarial nets, in: Z. Ghahramani, M. Welling, C. Cortes, N. D. Lawrence, K. Q. Weinberger (Eds.), Advances in Neural Information Processing Systems 27, Curran Associates, Inc., 2014, pp. 2672–2680.
- [36] L. Gatys, A. S. Ecker, M. Bethge, Texture synthesis using convolutional neural networks, in: C. Cortes, N. D. Lawrence, D. D. Lee, M. Sugiyama, R. Garnett (Eds.), Advances in Neural Information Processing Systems 28, Curran Associates, Inc., 2015, pp. 262–270.
- [37] D. R. Martin, C. C. Fowlkes, D. Tal, J. Malik, A database of human segmented natural images and its application to evaluating segmentation algorithms and measuring ecological statistics, Proceedings Eighth IEEE International Conference on Computer Vision. ICCV 2001 2 (2001) 416–423 vol.2.
- [38] J. Yang, J. Wright, T. S. Huang, Y. Ma, Image super-resolution via sparse representation, Trans. Img. Proc. 19 (11) (2010) 28612873. doi:10.1109/TIP.2010.2050625.
- [39] M. Bevilacqua, A. Roumy, C. Guillemot, M.-L. Alberi Morel, Low-Complexity Single-Image Super-Resolution based on Nonnegative Neighbor Embedding, in: British Machine Vision Conference (BMVC), Guildford, Surrey, United Kingdom, 2012.
URL <https://hal.inria.fr/hal-00747054>
- [40] R. Zeyde, M. Elad, M. Protter, On single image scale-up using sparse-representations, in: Proceedings of the 7th International Conference on Curves and Surfaces, Springer-Verlag, Berlin, Heidelberg, 2010, p. 711730. doi:10.1007/978-3-642-27413-8_47.
- [41] R. Timofte, V. D. Smet, L. V. Gool, A+: adjusted anchored neighborhood regression for fast super-resolution, in: D. Cremers, I. D. Reid, H. Saito, M. Yang (Eds.), Computer Vision - ACCV 2014 - 12th Asian Conference on Computer Vision, Singapore, Singapore, November 1-5, 2014, Revised Selected Papers, Part IV, Vol. 9006 of Lecture Notes in Computer Science, Springer, 2014, pp. 111–126. doi:10.1007/978-3-319-16817-3\8.
- [42] J. Huang, A. Singh, N. Ahuja, Single image super-resolution from transformed self-exemplars, in: IEEE Conference on Computer Vision and Pattern Recognition, CVPR 2015, Proceedings of the IEEE Computer Society

Conference on Computer Vision and Pattern Recognition, IEEE Computer Society, 2015, pp. 5197–5206. doi:10.1109/CVPR.2015.7299156.

- [43] Zhou Wang, A. C. Bovik, H. R. Sheikh, E. P. Simoncelli, Image quality assessment: from error visibility to structural similarity, *IEEE Transactions on Image Processing* 13 (4) (2004) 600–612. doi:10.1109/TIP.2003.819861.
- [44] D. P. Kingma, J. Ba, Adam: A method for stochastic optimization, CoRR abs/1412.6980.

Meenu Ajith received the bachelors degree in Electronics and Communication Engineering from Amrita school of Engineering in 2015 and the masters degree in 2017 in Electrical Engineering from The University of New Mexico in 2017. She is currently working towards her PhD degree in Electrical Engineering from The University of New Mexico. Her research interests are Machine Learning, Computer Vision, Pattern Recognition and Image Processing.

Aswathy Rajendra Kurup received the bachelors degree in Electronics and Communication Engineering from Amrita school of Engineering in 2015 and the masters degree in Electrical Engineering from The University of New Mexico in 2017. She is currently working towards her PhD degree in Electrical Engineering from The University of New Mexico. Her research interests are Image Processing, Signal Processing and Machine Learning.

Manel Martínez Ramón is a professor with the ECE department of The University of New Mexico. He holds the King Felipe VI Endowed Chair of the University of New Mexico, a chair sponsored by the Household of the King of Spain. He is a Telecommunications Engineer (Universitat Politecnica de Catalunya, Spain, 1996) and PhD in Communications Technologies (Universidad Carlos III de Madrid, Spain, 1999). His research interests are in Machine Learning applications to smart antennas, neuroimage, first responders and other cyber-human systems, smart grid and others. His last work is the monographic book *Signal Processing with Kernel Methods*, Wiley, 2018.